Research Article Vol. 10, No. 7 / 1 July 2020 / Optical Materials Express 1497
Optical Materials EXPRESS

Layer-by-layer spray coating of a stacked perovskite absorber for perovskite solar cells with better performance and stability under a humid environment

KOTH AMRATISHA,[1] JITPRABHAT PONCHAI,[1] PAPHADA KAEWURAI,[1] PIMSUDA PANSA-NGAT,[1] KUSUMA PINSUWAN,[1] PISIST KUMNORKAEW,[2] PIPAT RUANKHAM,[3,4] AND PONGSAKORN KANJANABOOS[1,5,*]

[1]*School of Materials Science and Innovation, Faculty of Science, Mahidol University, Bangkok 10400, Thailand*
[2]*National Nanotechnology Center (NANOTEC), Khlong Luang, Pathum Thani 12120, Thailand*
[3]*Department of Physics and Materials Science, Faculty of Science, Chiang Mai University, Chiang Mai 50200, Thailand*
[4]*Research Center in Physics and Astronomy, Faculty of Science, Chiang Mai University, Chiang Mai 50200, Thailand*
[5]*Center of Excellence for Innovation in Chemistry (PERCH-CIC), Ministry of Higher Education, Science, Research and Innovation, Bangkok 10400, Thailand*
[*]*Pongsakorn.kan@mahidol.edu*

Abstract: Perovskite is an emerging material for high performance solar cell application with low-cost solution-processable fabrication. As an ink, perovskite composition can be easily modified to create semi-transparent solar cells for window replacement. To enable scalable large-scale production, the spray process is one of the major candidates. In this work, we developed sequential spray deposition (SSD) to create double layer absorbers from different dimensional perovskites. SSD, for the first time, achieves layer-by-layer deposition of different perovskite materials for stacked architecture. To demonstrate the benefits, we spray-coated lower dimension, more stable perovskite onto high performance yet sensitive 3D semi-transparent perovskite. SSD performed under a humid environment (40 - 50% RH) brings about better film stability and retains good performance of 3D perovskite. Sequential spray deposition opens new routes for various stacking designs and large-scale production under economical ambient conditions.

1. Introduction

Organic-inorganic hybrid perovskite has become a good candidate for replacing conventional silicon solar cell due to its good properties such as strong light absorption coefficient, long carrier diffusion length, high carrier mobility and lifetime, bandgap tunability, and most importantly, low fabrication cost [1–6]. Typically, hybrid perovskite has formula of ABX_3 (for examples, $A = Cs^+$, CH_3N^{3+} (MA^+), $HC(NH_2)_2^+$ (FA^+); $B = Pb^{2+}$, Sn^{2+}, Ge^{2+}; $X = I^-$, Br^-, Cl^-). The common perovskite like $MAPbI_3$ for high efficiency requirement has dark color due to good visible light absorption [4]. However, in applications that require some transparency, mixed halide perovskite may be the solution. Bromine-iodide mixed halide perovskite, $MAPb(I_{1-x}Br_x)_3$ ($1>x>0$), has transparent, red appearance, which is the focus of this work [7–9]. When increasing x value (bromine doping), the bandgap enlarges as the color transforms from dark brown, red, to orange [7–9]. At the same time, PCEs of the perovskite solar cells decrease as they absorb less visible light [10]. Some transmission makes colored perovskite solar cells suitable for window

#391546 https://doi.org/10.1364/OME.391546
Journal © 2020 Received 28 Feb 2020; revised 27 Apr 2020; accepted 3 May 2020; published 3 Jun 2020

Optical Materials EXPRESS

replacement where power conversion is not the only criteria. Via spin coating under glovebox environment, researchers achieve 10.03% for red solar cells and 8.1% for orange bromide-rich perovskite solar cells [9,10]. To the best of our knowledge, there is currently no report on colored solar cell via scalable spray process.

$MAPbI_3$ perovskite lacks long-term stability under oxygen, humidity, heat, UV, and light illumination due to low formation energy; some of those externalities are typical environments of real-world solar cells operation [11–15]. One of the solutions is to replace MA with bulkier organic molecules such as PEA ($C_6H_5(CH_2)_2NH^{3+}$), creating layered perovskite or 2D Ruddlesden–Popper perovskite [16,17]. However, this type of perovskite suffers from low performance due to their low light absorption and poor carrier transport [18]. Alternatively, 2D/3D mixing or quasi-2D perovskite whose structure lays between 2D and 3D could be used to enhance stability of perovskite, while retaining good optoelectronic performance [18–20]. Reducing dimension effectively enlarges bandgap and changes its color [18]. Via spin coating of bulkier organic molecules in IPA onto 3D perovskite, thin 3D perovskite at the surface could be converted to be a 2D capping layer, correcting surface/grain boundary imperfection and reducing trap-state densities due to cationic, and halide vacancies [21]. The 2D/3D stacking structure from similar surface treatment strategy can also promote thermal stability as larger organic separation in 2D perovskite better suppresses ion migration at high temperature [22,23].

In contrast to spin process mentioned above, spray process can be used to fabricate perovskite thin film on large substrate, allowing commercial scale production. In early work, spray coating was only used in the second deposition step after spin coating of PbI_2. The spray-assisted fabrication replaces dripping process by spraying MAI solution directly on the dried PbI_2 thin-film, improving surface morphology, and promoting efficiency from 10.9% to 12.5% [24]. In later works, spray process was applied to the whole perovskite formation i.e. one step deposition of $MAPbI_3$ precursor solution. As substrates are heated during spray process, when precursor solution droplets reach the hot substrates, they dry immediately, leading to better surface morphology from faster and uniform crystallization [25]. Optimal inward flux (precursor solution), and outward flux (solvent evaporation) during spray deposition can enlarge grain size of perovskite thin-film, promoting charge transportation, and improving performance [26]. The optimization can be achieved by varying spray parameters such as spray rate, $MAPbI_3$ solution concentration, solvent, spray height, and substrate temperature, yielding black perovskite solar cells with PCE of 16.68% [27]. Another approach to achieve black $MAPbI_3$ film from spray process is re-dissolution, which promotes reaction between $PbCl_2$ and MAI (1:3 ratio) dissolved in IPA. As $MAPbI_3$ does not dissolve well in IPA, tiny perovskite crystals are precipitated out with high yield. These crystals were then dried, and dissolved in DMF/GBL for spray deposition, achieving average PCE of 16.08% [26].

To demonstrate colored perovskite solar cell via spray coating under ambient environment for window replacement application, in this work, we instead focused on mixed halide perovskite, $MAPbBr_2I$, with red, transparent feature. We developed sequential spray deposition (SSD) where two dimensional perovskites were sprayed consecutively onto a pre-heated substrate. In contrast, for the traditional spin coating, the lower perovskite layer would be affected by solvent used during the deposition of the second layer perovskite, which causes inhomogeneous interlayer and resulting in lower performance from non-radiative recombination, [28–30] explaining why 2D/3D stacking structure was previously achieved by surface treatment of 3D perovskite [21,22,31,32]. However, with the nature of spray process where tiny spray droplets quickly dried on a hot substrate, second-layer solution (Quasi-2D) immediately evaporates and crystalized on top of the first layer (3D perovskite) upon contact, avoiding the formation of high defects interlayer. SSD, for the first time, enables deposition of perovskite materials specifically for each layer; additionally, thickness of each layer can be selected and optimized unlike previous surface passivation methods. Double layer perovskite via SSD combines long diffusion length, low

Optical Materials EXPRESS

binding energy, and high performance of n = ∞ (3D) with stability of n50 (quasi-2D) perovskite, achieving better performance compared to 3D or Quasi-2D perovskite alone. It was reported that the applying n1 perovskite can be a promising strategy to solve stability problems of 3D perovskite as shown a better humidity tolerance. Unfortunately, their high exciton energy and large band gap affect on charge transportation ability caused lower efficiency [33–35]. As a sequence, a reducing of the large organic ligand layer that fitted perovskite in to layers can reduce the exciton binding energy and simultaneous lower the band gap, besides it can still enhance the humidity resistance [4,21,36,37]. We investigated and optimized different spray parameters for efficient and stable red-colored perovskite solar cell under ambient environments.

2. Experimental

Lead bromide ($PbBr_2$; 98% purity), anhydrous N,N-dimethylformamide (DMF; 99.8% v/v), anhydrous gamma-butyrolactone (GBL; 99%), anhydrous ethanol (99.5%), titanium(IV) isopropoxide (TTIP; 99.999%), and hydrochloric acid (HCl; 37% v/v) were purchased from Sigma-Aldrich. Phenethylammonium iodide (PEAI) and methylammonium iodide (MAI) were purchased from Dyesol.

Fluorine-doped tin oxide (FTO) coated glass substrates were cleaned by ultrasonic cleaning in soap water followed by deionized water, and isopropanol. After that, the substrates were soaked in isopropanol overnight and dry with blowing N_2 gas before treated with an UV–ozone cleaner prior to all the experiments. TiO_2 solution was prepared by dropping 780 uL of TTIP dropwise into 8 mL of anhydrous ethanol while stirring with a magnetic stirrer. Then 60 uL of concentrated HCl was added dropwise while stirring. The solution was stirred at room temperature overnight, then spin coated on FTO substrate with 2,000 rpm spin speed, and 1,000 rpm/s acceleration. Then, the substrates were heated at 125°C for 15 minutes, 255°C for 15 minutes, 375°C for 15 minutes, and 520°C for 1 hour. After reaching the room temperature, the substrates were soaked in 0.12 M $TiCl_4$ solution at 70°C for 30 minutes before washed with distilled water, and dried with N_2 gas. Lastly, the substrates were annealed on hotplate at 520°C for 2 hours.

Dimensional mixed halide perovskite solutions, $(PEA)_2(MA)_{n-1}Pb_nI_{n+1}Br_{2n}$ (0.4 M, n = 1, 5, 50, and ∞), were prepared in DMF (n = 1, 5, and 50) and DMF : GBL = 8 : 2 (n = ∞ or 3D). PEAI, MAI, and $PbBr_2$ powders with molar ratio of 2 : n-1 : n were used, respectively. The solution was stirred at 70°C for at least 30 minutes or until completely dissolved under glovebox environment before filtering with PTFE syringe filter (Whatman, 0.22 mm).

Airbrushes (Badger 200 series connected to N_2 gas with 30 psi pressure) under ambient environment (40–50% RH) were utilized. For all spray depositions, substrates were pre-heated to 100°C prior to and during spray deposition. For single layer perovskite deposition, we used a single airbrush with spray rate of 50 μL/s and 0.4 M solution, having a similar setup to Fig. 2(b). After the deposition, the film was annealed at 100°C for 20 minutes to be fully crystallized. For sequential spray deposition (multilayer perovskite), we used two airbrushes setup as shown in Fig. 2(b) with spray rate of 50 μL/s and 0.4 M solution. After depositing the first layer, the film was heated at 100°C for 30 seconds to dry out the remaining solvent. Then, the second layer was coated on top. The double-layer film was then annealed at 100°C for 20 minutes.

Spiro-OMeTAD solution was prepared by mixing 80 mg of Spiro-OMeTAD in 1 mL of chlorobenzene at room temperature for 1 hour. 28.5 uL of 4-*tert*-butylpyridine and 17.5 uL of Li-TFSI solution (520 mg/mL in chlorobenzene) were added and stirred overnight. The solution was dropped on a substrate and rested for 30 seconds before spin coating with spin speed of 2,000 rpm and acceleration of 1,000 rpm/s. Finally, the film was left to oxidize in a desiccator overnight before depositing gold electrode (100 nm thick, 0.02 nm/s deposition rate) through thermal evaporation.

Surface morphologies were tested by scanning electron microscopy (SEM; Quanta 450 FEI, Tungsten filament electron source, 20 kV, secondary electron mode). The optical absorption

Optical Materials EXPRESS

spectra were recorded by a Shimadzu UV-2600 UV-Vis spectrophotometer (300–800 nm, Slow mode, absorbance mode). The crystal structure was characterized by an DKSH Aeris benchtop X-Ray Diffractometer (Cu anode material, detector scan mode using step size of 0.0217 degree, 3.515 seconds per step, and 2 theta starts from 4 to 55 degree). Photoluminescence were recorded by Horiba FluoroMax4+ spectrofluorometer (Integration time of 0.1 s, excitation of 410 nm, excitation slit of 15 nm, emission wavelength measurement between 450 and 780 nm, and emission slit of 10 nm). Solar cell parameters including I-V curve were measured by Keithley 2400 source meter. Perovskite solar cell samples were exposed to 1 sun illumination during the measurements.

3. Results and discussion

For spray-coated single layer perovskite thin films shown in Fig. 1(a), (n)∞ perovskite ($MAPbIBr_2$) starts to absorb at 637 nm corresponding to the bandgap energy of 1.94 eV, similar to that of the quasi-2D perovskite (n50). We observed a small kink at 540 nm from n50 perovskite caused by $MAPbBr_3$ formation in the sample [38,39]. At high n values, bandgap energies of quasi-2D perovskites are similar to those of 3D perovskite; at low n values ($1 \leq n \leq 10$), bandgap energies are dramatically enlarged due to quantum effect of reduced dimension [18,40]. Absorption edges of n1 and n5 samples shift towards shorter wavelengths at 489 and 606 nm, corresponding to the bandgap energies of 2.54 and 2.05 eV, respectively. The addition of aromatic organic cations causes quantum confinement in the perovskite materials, blue-shifting the bandgap energies and leading to different colors; n∞ (3D), n50, n30, n10, n5, and n1 perovskites have red, lighter red, to yellow colors as shown in Fig. 1(d). n∞ to n30 have a similar color.

XRD peaks of $MAPbI_3$ are located at 14.02°, 19.98°, 23.38°, 24.42°, 28.38°, 31.83°,34.92°, 40.53°, and 43.08°, corresponding to the (110), (112), (211), (202), (220), (310), (312), (224), and (314) crystal planes of the tetragonal phase [41]. We observed the diffraction peaks of $MAPbIBr_2$ (n∞) at 14.63°, 20.74°, and 29.48°. Tiny PbI_2 peaks appear in n50 and n5 perovskite films. This may indicate the increasing of x value in $MAPb(I_{1-x}Br_x)_3$, slightly shifting XRD peaks towards larger angles i.e. n∞ has the (110) plane peak at 14.63° compared to the $MAPbI_3$ peak at 14.02° while n50 and n5 have their peaks at 14.74° and 14.83°, respectively [42].

In Fig. 1(c), PL results indicate different phases of perovskite within thin-films from spray deposition of different calcuated dimensions. With lower dimension, the magnitude of the main PL peak at 735 nm, which is slightly blueshifted from 765 nm of typical $MAPbI_3$ [43] perovskite due to Br doping, reduces with the increasing of the peak at 630 nm. At n=1, the single main peak is located at 490 nm. The appearance of PL peaks at lower wavelength relates to the emission from 2D perovskite components [44] i.e. $(PEA)_2(MA)_4Pb_5I_6Br_{12}$ (n5) with emission around 630 nm. With lower demension, the compositions are shifted towards more population of 2D components, explaining the superior stability.

With different dimensionality, perovskites differ in band energies and stability characteristics. To achieve beneficial combinations, we focused on double layer perovskite solar cells where n50 with higher stability [16,18,22,38,45] compared to n∞ (3D) perovskite was deposited as a capping layer. In this work, double layer n∞/n50 perovskite solar cells were fabricated via sequential spray deposition as shown in Fig. 2(b). We optimized thicknesses of both perovskite layers (see Fig. 5.) to maximize the performance. From Fig. 2(a), double layer perovskite has similar absorption to n∞ and n50 perovskites. All three conditions have average visible transmittances about 45% (see Table 2 in the appendix). The bump at 540 nm does not appear for n∞/n50 perovskite, most likely because the capping layer is very thin [22,46].

From SEM cross-section in Fig. 2(d), both perovskite layers inside the double layer perovskite solar cells can be seen. The thickness of the capping layer (n50) is around 90 nm with spray time of 2 seconds, and deposition rate of 45 nm/s. The n∞ (3D) perovskite layer was fabricated with 9 seconds of spray deposition, resulting in 400 nm thickness, and similar deposition rate of around

Optical Materials EXPRESS

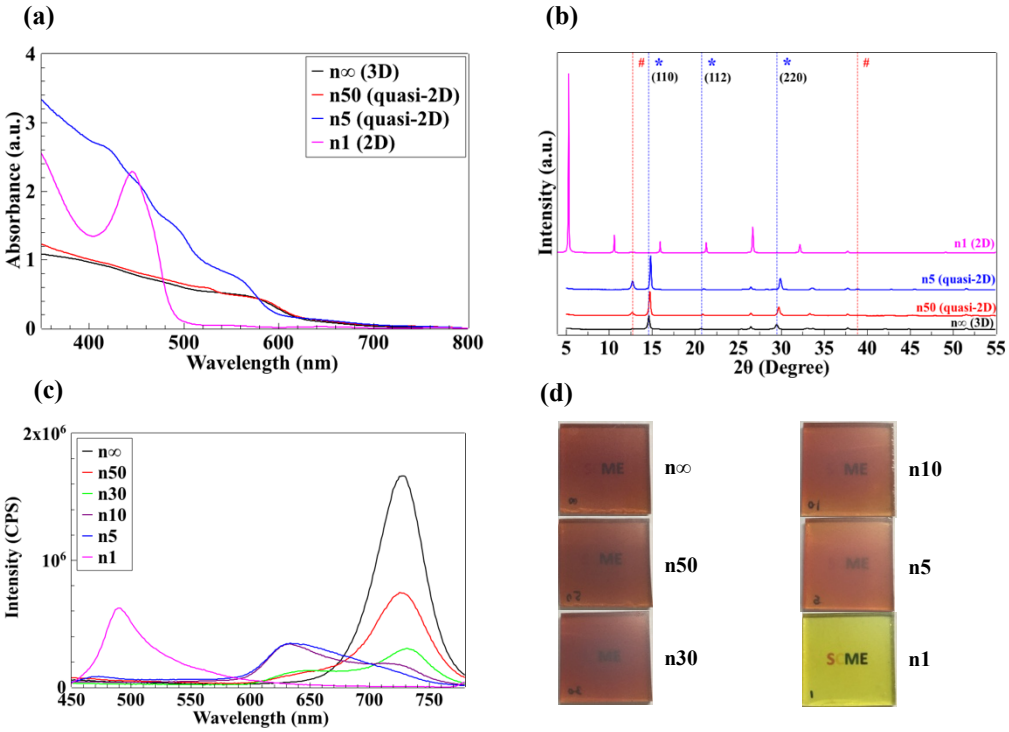

Fig. 1. (a) UV-Vis absorption of n∞ (3D), n50 (quasi-2D), n5 (quasi-2D), and n1 (2D) perovskite thin films. The film colors are changed according to dimensionality. (b) X-ray diffraction peaks of perovskite thin films (labeled with *) with different dimensions. PbI_2 peaks are labeled with #. (c) Photoluminescence spectra (PL) of n∞, n50, n30, n10, n5, and n1 perovskite thin films. (d) Optical images of n∞, n50, n30, n10, n5, and n1 perovskite thin films.

44 nm/s (see Fig. 6 for additional information). From Fig. 2(d), the distinction between n∞, and n50 layer can be clearly observed, confirming sharp interface between main, and capping layers. As shown from SEM top surfaces in Fig. 2(d), both n∞ and n50 thin films via spray deposition with the same thickness about 400 nm have large grains with distinctly different surface features. However, morphology changes with thickness [27,48]. As a 90-nm-thick capping layer, n50 has favorable small grains; depositing it on top of n∞ perovskite helped fill up surface pinholes and increase coverage (see Fig. 7).

X-ray diffraction of n∞, n∞/n50, and n50 perovskites are shown in Fig. 3(b). There is a small peak corresponding to PbI_2 in n50 perovskite sample. However, we did not observe this peak for n∞/n50 perovskite due to thin capping layer. Small shift to larger 2θ for n∞/n50 indicates successful double deposition in agreement with the SEM results. In term of crystallinity, n∞/n50 has lower crystallite size, as smaller n50 grains pack on top of n∞ surface (see Fig. 7 and Table 2 in the appendix).

As shown in in Fig. 3(b), after 500 hours exposure to humidity, all perovskite films have lower absorption with new $MAPbBr_3$ absorption peak appearing at 525 nm, which indicates the partial transformation from $MAPb(I_{1-x}Br_x)_3$ to $MAPbBr_3$ [38,39]. However, n∞ and n50 perovskites show better stability by retaining similar values of absorption. In Fig. 3(d), higher contact angles for n∞/n50, and n50 films further direct to better water repellences and moisture resistance [21,49]. Highest contact angle for n∞/n50 supports better surface coverage [21] as the second spray deposition can smooth out morphological defects in the lower layer. In term of heat

Optical Materials EXPRESS

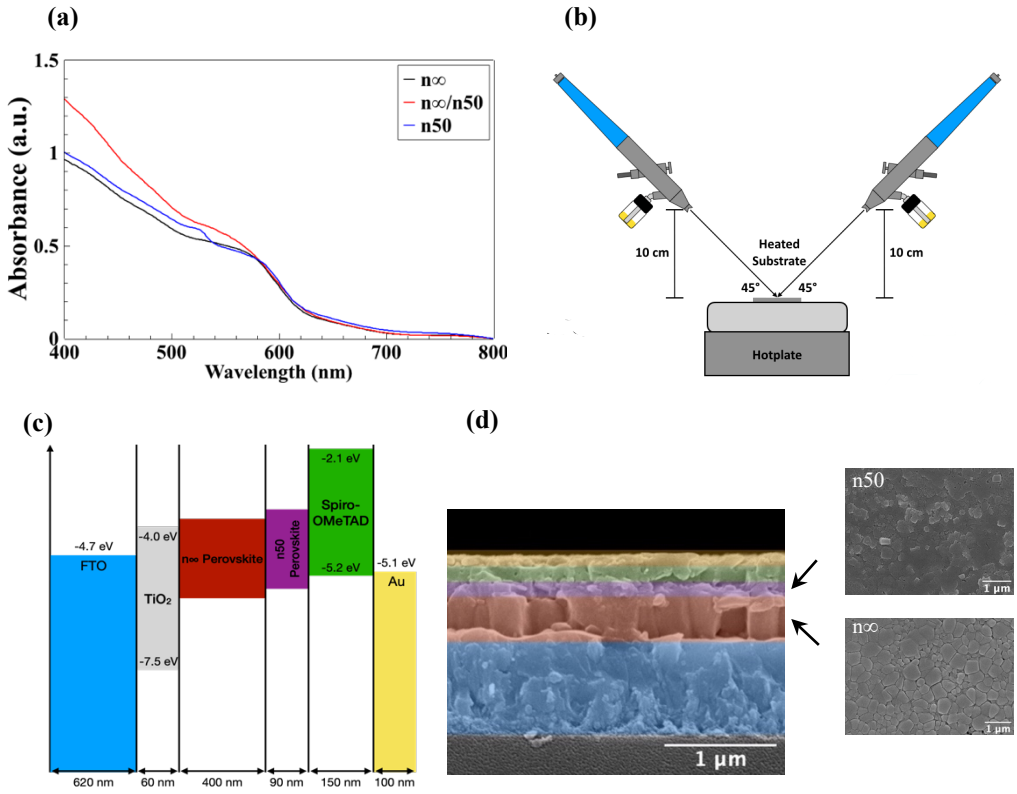

Fig. 2. (a) UV-Vis absorption of single layer (n∞, n50) and double layer n∞/n50 perovskite thin films. (b) Spray setup used for depositing double layer perovskite thin film. (c) Band diagram of double layer n∞/n50 perovskite solar cell versus thickness of each layer of the device. [47] (d) SEM cross-section of different layers in n∞/n50 perovskite solar cell and top surfaces of n∞ and n50 thin films. Top surface images are from two single layer samples both with thickness around 400 nm.

stability, n∞/n50, and n50 films turn yellow slower than n∞ (3D) alone did, indicating better heat tolerance as shown in Fig. 3(c). The increasing of heat resistance can be explained by PEAI content in perovskite film [21]. In agreement with previous work [22], the capping layer could boost thermal stability by suppressing MA^+ or halide volatilization from the n∞ (3D) layer as PEA^+ volatilization or PEA^+/inner MA^+ exchange is not favorable.

Figure 4(a) shows box plot from n∞, n∞/n50, and n50 perovskite solar cell statistics (Table 3). The box indicates first, second and third quartile with top and bottom line indicating 5% and 95% PCEs. The x mark indicates maximum and minimum PCEs. We achieved 3.32% maximum power conversion efficiency (PCE) of semi-transparent red perovskite solar cells (average visible transmittance of 43%) fabricated with SSD fabricated under humid environment (40 -50% RH). Figure 4(b) shows J_{sc} and V_{oc} of n∞, n∞/n50, and n50 perovskite solar cells with standard deviation. From Table 1 and Fig. 4(a), we observed slight improvement in average PCE from 2.26% for n∞ to 2.70% for n∞/n50 with lower standard deviation. The similar performance is expected as the majority of double layer perovskite is n∞. Higher J_{sc} and FF may be related to reduction of surface recombination due to PEA surface passivation [50] and better film uniformity as n50 fills up surface defects of the lower n∞ layer.

Optical Materials EXPRESS

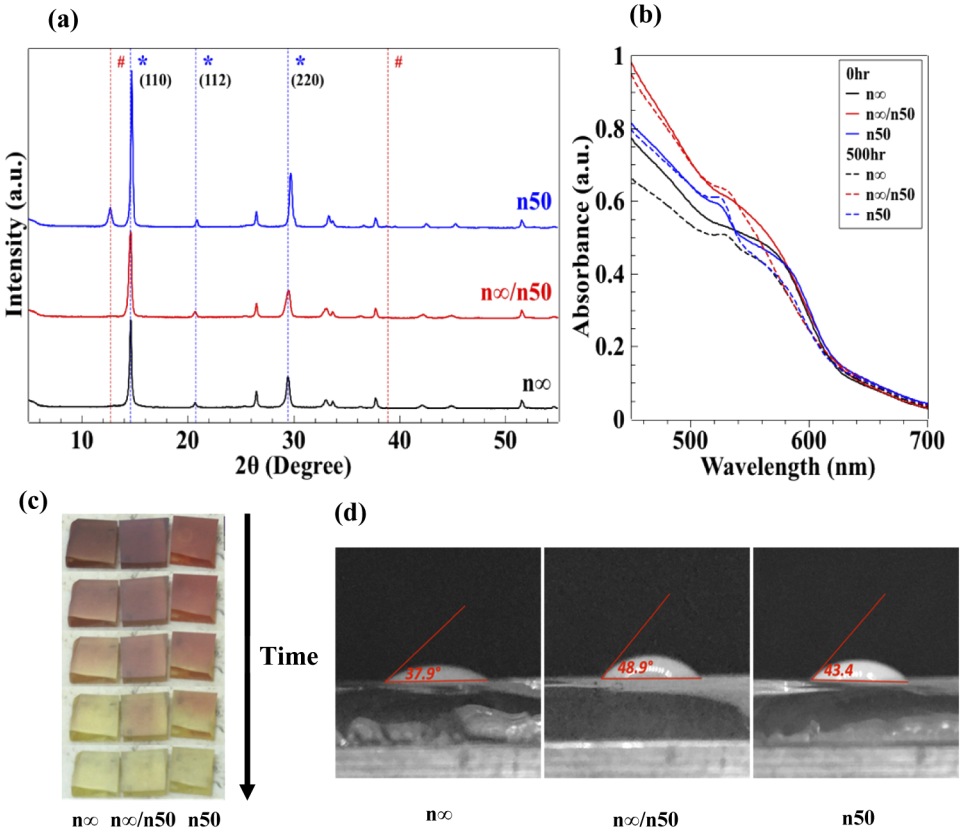

Fig. 3. (a) X-ray diffraction peaks of perovskite thin films (labeled with *) with different dimensions. PbI_2 peaks are labeled with #. (b) UV-Vis spectroscopy of n∞, n∞/n50, and n50 perovskite before and after 500 hours under 50% RH. (c) Perovskite films heated at 300°C captured 1 minute apart for each frame. (d) Contact angles of distilled water (20 μL droplet) on top of perovskite films.

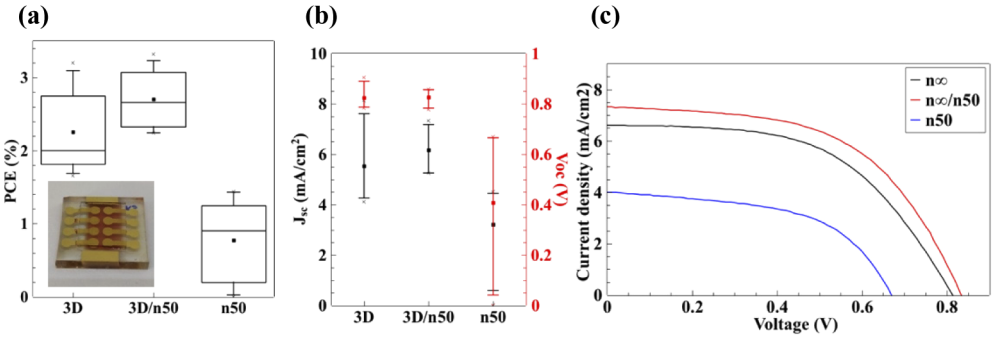

Fig. 4. (a) Power conversion efficiency (PCE), (b) J_{sc} and V_{oc}, (c) J-V curve of n∞, n∞/n50, and n50 perovskite solar cells.

Optical Materials EXPRESS

Table 1. Average solar cell parameters of n∞, n∞/n50, and n50 perovskite solar cells.

	PCE (%)	J_{sc} (mA/cm^2)	V_{oc} (V)	FF	R_{sh} (Ω cm^2)	R_s (Ω cm^2)
n∞	2.26	5.54	0.83	0.49	1979	53.38
n∞/n50	2.70	6.17	0.83	0.53	1296	37.94
n50	0.77	3.21	0.41	0.39	766	34.08

4. Conclusions

With the aim for scalable perovskite process, we developed sequential spray deposition, which, for the first time, allows layer-by-layer perovskite deposition to create multi-layer perovskite absorber. Choosing semi-transparent perovskite system to demonstrate SSD, we deposited mixed halide quasi-2D perovskite (n50) on top of 3D perovskite (n∞). Combing the stability of layered system, and the performance of 3D system, n∞/n50 double layer perovskite earns both features crucial for commercial application. As a deposition process, SSD is applicable to various perovskite recipes and multi-layer designs.

Appendix

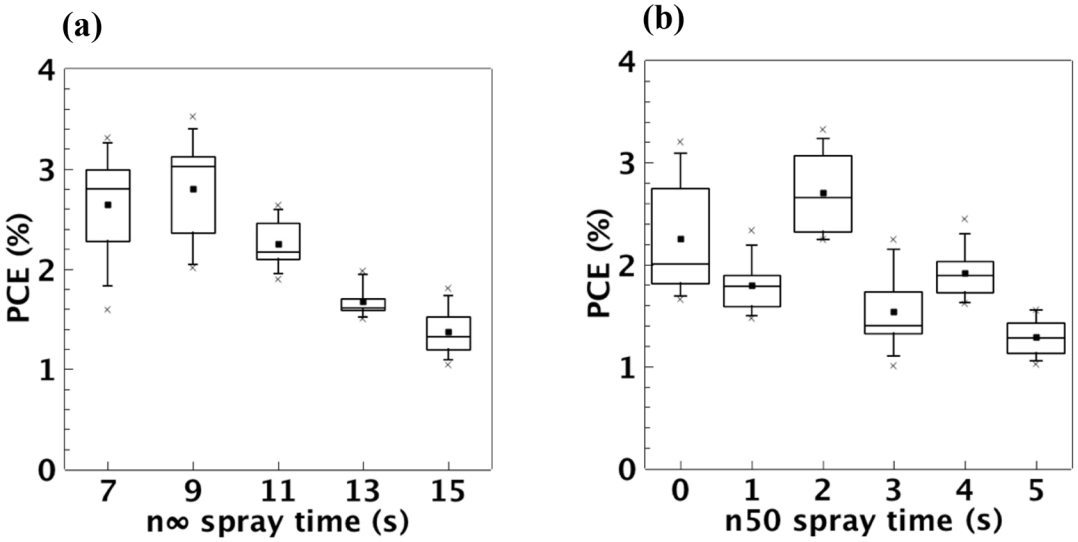

Fig. 5. (a) PCEs of double layer n∞/n50 perovskite solar cell with various n∞ spray times. Spray time of n50 capping layer was fixed at 2 seconds for all samples. (b) PCE of n∞/n50 perovskite solar cell with 9 seconds n∞ perovskite spray time, and various n50 spray times.

Table 2. Average crystallite sizes of n∞, n∞/n50, and n50 perovskite calculated from (110) and (220) planes and average visible transmittance (AVT).

Sample	Crystallite size (nm)		AVT(%)
	(110)	(220)	
n∞	36.02	22.21	46.38
n∞/n50	26.92	16.15	43.00
n50	42.63	28.35	44.32

Optical Materials EXPRESS

Table 3. Solar cell parameters from 8 devices for n∞, n∞/n50, and n50 perovskite solar cells under 1 sun illumination.

Sample	PCE (%)	J_{sc}(mA/cm^2)	V_{oc}(V)	FF	R_{sh}(Ω·cm^2)	R_s(Ω·cm^2)
n∞	1.842	4.550	0.905	0.447	1404	89.49
	1.756	4.527	0.833	0.466	1458	73.91
	2.003	4.962	0.863	0.467	1134	68.73
	1.655	4.107	0.816	0.494	1415	67.51
	2.893	6.597	0.813	0.539	4887	37.08
	1.998	4.798	0.783	0.532	1525	48.80
	3.203	8.135	0.796	0.494	1451	33.30
	2.700	6.639	0.792	0.514	2555	40.21
Average	2.26	5.54	0.83	0.49	1979	57.38
n∞/n50	2.719	6.368	0.858	0.498	1706	45.90
	2.596	6.204	0.852	0.491	176	47.38
	2.243	5.243	0.833	0.513	2391	49.32
	3.066	6.889	0.831	0.535	1211	32.12
	2.248	5.268	0.777	0.549	1176	34.77
	2.354	5.454	0.794	0.544	1391	35.84
	3.072	6.624	0.833	0.557	1085	28.87
	3.321	7.330	0.834	0.543	1229	29.35
Average	2.70	6.17	0.83	0.53	1296	37.94
n50	1.19	4.51	0.512	0.516	953	24.95
	0.24	4.36	0.206	0.272	55	34.76
	1.19	4.18	0.540	0.525	2157	29.37
	0.00	0.00	0.000	0.000	0	0.00
	1.44	4.00	0.669	0.538	947	30.50
	1.42	4.14	0.659	0.521	753	33.82
	0.62	2.75	0.551	0.409	815	68.98
	0.07	1.73	0.118	0.325	453	50.27
Average	0.77	3.21	0.41	0.39	766	34.08

Optical Materials EXPRESS

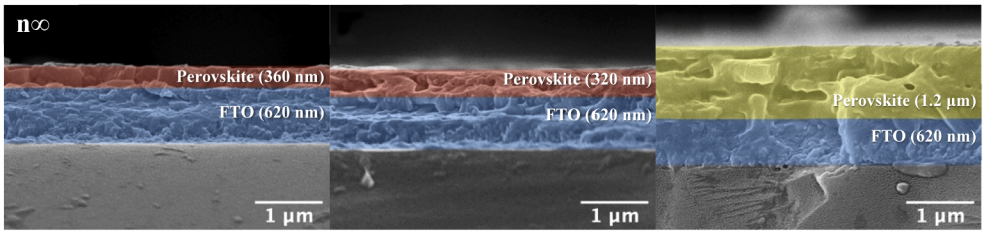

Fig. 6. SEM cross-sections of n∞, n5 (quasi-2D), and n1(2D) perovskite thin films. All perovskite films were deposited with 50 μL/s spray rate, 4 seconds spray time, and 0.2 M solution in DMF.

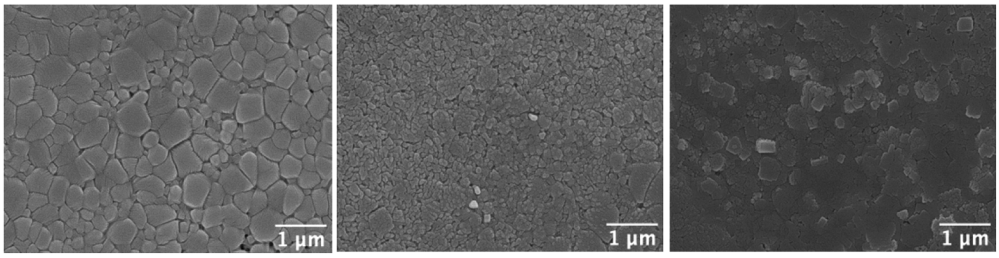

Fig. 7. SEM surface morphology of (a) 3D, (b) 3D/quasi-2D (n50), and (c) quasi-2D (n50) perovskites.

Funding

EGAT & NSTDA (FDA-CO-2560-5449- TH); Thailand Research Fund & OHEC (MRG61-80282); Research Fund for DPST Graduate with First Placement (#005/ 2558); Faculty of Science, Mahidol University (CIF Grant); Energy Policy and Planning Office, Ministry of Energy (funding for higher education students); Center of Excellence for Innovation in Chemistry (PERCH-CIC); Ministry of Higher Education, Science, Research and Innovation.

Acknowledgements

We acknowledge fruitful discussions and assistance from Dr. Tanakorn Osotchan, Dr. Pasit Pakawatpanurut, Atittaya Naikaew, Ladda Srathongsian, Kwanchai Peanpong, Zoubeir Saraw, Teepich Houtae, Khine Zin Swe, Myo Zin Tun, and Jaruwan Yakiangngam.

Disclosures

The authors declare no conflicts of interest.

References

1. H. S. Jung and N. G. Park, "Perovskite solar cells: From materials to devices," Small **11**(1), 10–25 (2015).
2. S. A. Veldhuis, P. P. Boix, N. Yantara, M. Li, T. C. Sum, N. Mathews, and S. G. Mhaisalkar, "Perovskite materials for light-emitting diodes and lasers," Adv. Mater. **28**(32), 6804–6834 (2016).
3. J. S. Shaikh, N. S. Shaikh, A. D. Sheikh, S. S. Mali, A. J. Kale, P. Kanjanaboos, C. K. Hong, J. H. Kim, and P. S. Patil, "Perovskite solar cells: In pursuit of efficiency and stability," Mater. Des. **136**, 54–80 (2017).
4. P. P. Boix, S. Agarwala, T. M. Koh, N. Mathews, and S. G. Mhaisalkar, "Perovskite solar cells: Beyond methylammonium lead iodide," J. Phys. Chem. Lett. **6**(5), 898–907 (2015).
5. M. Afzaal and H. M. Yates, "Growth patterns and properties of aerosol-assisted chemical vapor deposition of $CH_3NH_3PbI_3$ films in a single step," Surf. Coat. Technol. **321**, 336–340 (2017).
6. S. Pramchu, A. P. Jaroenjittichai, and Y. Laosiritaworn, "Surface doping of Sn in orthorhombic $CH_3NH_3PbI_3$ for potential perovskite solar cells: first principles study," Surf. Coat. Technol. **306**, 285–289 (2016).
7. P. Luo, Y. Zhou, W. Xia, S. Zhou, J. Liu, Y. Lu, C. Xu, and L. Sun, "Colorful, bandgap-tunable, and air-stable $CsPb(I_xBr_{1-x})_3$ inorganic perovskite films via a novel sequential chemical vapor deposition," Ceram. Int. **44**(11), 12783–12788 (2018).

Optical Materials EXPRESS

8. J. Ponchai, P. Kaewurai, C. Boonthum, K. Pinsuwan, T. Supasai, S. Sahasithiwat, and P. Kanjanaboos, "Modifying morphology and defects of low-dimensional, semi-transparent perovskite thin films: Via solvent type," RSC Adv. **9**(21), 12047–12054 (2019).
9. Z. Fang and Z. Yi, "First principles study on mixed orthorhombic perovskite $CH_3NH_3Pb(I_{1-x}Br_x)_3$," Chem. Phys. Lett. **687**, 19–22 (2017).
10. L. Yuan, Z. Wang, R. Duan, P. Huang, K. Zhang, Q. Chen, N. K. Allam, Y. Zhou, B. Song, and Y. Li, "Semi-transparent perovskite solar cells: Unveiling the trade-off between transparency and efficiency," J. Mater. Chem. A **6**(40), 19696–19702 (2018).
11. U. Mehmood, A. Al-Ahmed, M. Afzaal, F. A. Al-Sulaiman, and M. Daud, "Recent progress and remaining challenges in organometallic halides based perovskite solar cells," Renewable Sustainable Energy Rev. **78**, 1–14 (2017).
12. Q. M. Hong, R. P. Xu, T. Y. Jin, J. X. Tang, and Y. Q. Li, "Unraveling the light-induced degradation mechanism of $CH_3NH_3PbI_3$ perovskite films," Org. Electron. **67**, 19–25 (2019).
13. M. Ouafi, B. Jaber, L. Atourki, R. Bekkari, and L. Laânab, "Improving UV stability of $MAPbI_3$ perovskite thin films by bromide incorporation," J. Alloys Compd. **746**, 391–398 (2018).
14. K. Pinsuwan, C. Boonthum, T. Supasai, S. Sahasithiwat, P. Kumnorkaew, and P. Kanjanaboos, "Solar perovskite thin films with enhanced mechanical, thermal, UV, and moisture stability via vacuum-assisted deposition," J. Mater. Sci. **55**(8), 3484–3494 (2020).
15. A. Buin, P. Pietsch, J. Xu, O. Voznyy, A. H. Ip, R. Comin, and E. H. Sargent, "Materials processing routes to trap-free halide perovskites," Nano Lett. **14**(11), 6281–6286 (2014).
16. I. C. Smith, E. T. Hoke, D. Solis-Ibarra, M. D. McGehee, and H. I. Karunadasa, "A layered hybrid perovskite solar-cell absorber with enhanced moisture stability," Angew. Chem. Int. Ed. **53**(42), 11232–11235 (2014).
17. D. H. Cao, C. C. Stoumpos, O. K. Farha, J. T. Hupp, and M. G. Kanatzidis, "2D homologous perovskites as light-absorbing materials for solar cell applications," J. Am. Chem. Soc. **137**(24), 7843–7850 (2015).
18. L. N. Quan, M. Yuan, R. Comin, O. Voznyy, E. M. Beauregard, S. Hoogland, A. Buin, A. R. Kirmani, K. Zhao, A. Amassian, D. H. Kim, and E. H. Sargent, "Ligand-stabilized reduced-dimensionality perovskites," J. Am. Chem. Soc. **138**(8), 2649–2655 (2016).
19. A. Naikaew, P. Kumnorkaew, T. Supasai, S. Suwanna, R. Hunkao, T. Srikhirin, and P. Kanjanaboos, "Enhancing high humidity stability of quasi-2D perovskite thin films through mixed cation doping and solvent engineering," ChemNanoMat **5**(10), 1280–1288 (2019).
20. K. Z. Swe, A. Naikaew, P. Kaewurai, P. Pansa-Ngat, S. Sahasithiwat, L. Kangkaew, S. Rugmai, S. Soontaranon, and P. Kanjanaboos, "Layered perovskite with compact morphology and reduced grain size via vacuum assisted crystallization for luminescence applications," Opt. Mater. Express **10**(5), 1182 (2020).
21. T. M. Koh, V. Shanmugam, X. Guo, S. S. Lim, O. Filonik, E. M. Herzig, P. Müller-Buschbaum, V. Swamy, S. T. Chien, S. G. Mhaisalkar, and N. Mathews, "Enhancing moisture tolerance in efficient hybrid 3D/2D perovskite photovoltaics," J. Mater. Chem. A **6**(5), 2122–2128 (2018).
22. Y. Lin, Y. Bai, Y. Fang, Z. Chen, S. Yang, X. Zheng, S. Tang, Y. Liu, J. Zhao, and J. Huang, "Enhanced thermal stability in perovskite solar cells by assembling 2D/3D stacking structures," J. Phys. Chem. Lett. **9**(3), 654–658 (2018).
23. Y. Lin, Y. Bai, Y. Fang, Q. Wang, Y. Deng, and J. Huang, "Suppressed ion migration in low-dimensional perovskites," ACS Energy Lett. **2**(7), 1571–1572 (2017).
24. F. Li, C. Bao, H. Gao, W. Zhu, T. Yu, J. Yang, G. Fu, X. Zhou, and Z. Zou, "A facile spray-assisted fabrication of homogenous flat $CH_3NH_3PbI_3$ films for high performance mesostructure perovskite solar cells," Mater. Lett. **157**, 38–41 (2015).
25. M. Ramesh, K. M. Boopathi, T. Y. Huang, Y. C. Huang, C. S. Tsao, and C. W. Chu, "Using an airbrush pen for layer-by-layer growth of continuous perovskite thin films for hybrid solar cells," ACS Appl. Mater. Interfaces **7**(4), 2359–2366 (2015).
26. J. H. Heo, M. H. Lee, M. H. Jang, and S. H. Im, "Highly efficient $CH_3NH_3PbI_{3-x}Cl_x$ mixed halide perovskite solar cells prepared by re-dissolution and crystal grain growth via spray coating," J. Mater. Chem. A **4**(45), 17636–17642 (2016).
27. H. Chen, X. Ding, X. Pan, T. Hayat, A. Alsaedi, Y. Ding, and S. Dai, "Comprehensive studies of air-brush spray deposition used in fabricating high-efficiency $CH_3NH_3PbI_3$ perovskite solar cells: Combining theories with practices," J. Power Sources **402**, 82–90 (2018).
28. M. A. Mahmud, T. Duong, Y. Yin, H. T. Pham, D. Walter, J. Peng, Y. Wu, L. Li, H. Shen, N. Wu, N. Mozaffari, G. Andersson, K. R. Catchpole, K. J. Weber, and T. P. White, "Double-sided surface passivation of 3D perovskite film for high-efficiency mixed-dimensional perovskite solar cells," Adv. Funct. Mater. **30**(7), 1907962 (2020).
29. J. P. Correa-Baena, W. Tress, K. Domanski, E. H. Anaraki, S. H. Turren-Cruz, B. Roose, P. P. Boix, M. Grätzel, M. Saliba, A. Abate, and A. Hagfeldt, "Identifying and suppressing interfacial recombination to achieve high open-circuit voltage in perovskite solar cells," Energy Environ. Sci. **10**(5), 1207–1212 (2017).
30. M. Stolterfoht, C. M. Wolff, J. A. Márquez, S. Zhang, C. J. Hages, D. Rothhardt, S. Albrecht, P. L. Burn, P. Meredith, T. Unold, and D. Neher, "Visualization and suppression of interfacial recombination for high-efficiency large-area pin perovskite solar cells," Nat. Energy **3**(10), 847–854 (2018).

Optical Materials EXPRESS

31. Z. Wang, Q. Lin, F. P. Chmiel, N. Sakai, L. M. Herz, and H. J. Snaith, "Efficient ambient-air-stable solar cells with 2D-3D heterostructured butylammonium-caesium-formamidinium lead halide perovskites," Nat. Energy **2**(9), 17135 (2017).
32. S. Gharibzadeh, B. Abdollahi Nejand, M. Jakoby, T. Abzieher, D. Hauschild, S. Moghadamzadeh, J. A. Schwenzer, P. Brenner, R. Schmager, A. A. Haghighirad, L. Weinhardt, U. Lemmer, B. S. Richards, I. A. Howard, and U. W. Paetzold, "Record open-circuit voltage wide-bandgap perovskite solar cells utilizing 2D/3D Perovskite Heterostructure," Adv. Energy Mater. **9**(21), 1803699 (2019).
33. W. Fu, J. Wang, L. Zuo, K. Gao, F. Liu, D. S. Ginger, and A. K.-Y. Jen, "Two-dimensional perovskite solar cells with 14.1% power conversion efficiency and 0.68% external radiative efficiency," ACS Energy Lett. **3**(9), 2086–2093 (2018).
34. F. Zhang, H. Lu, J. Tong, J. J. Berry, M. C. Beard, and K. Zhu, "Advances in two-dimensional organic–inorganic hybrid perovskites," Energy Environ. Sci. **13**(4), 1154–1186 (2020).
35. H. Zheng, D. Liu, Y. Wang, Y. Yang, H. Li, T. Zhang, H. Chen, L. Ji, Z. Chen, and S. Li, "Synergistic effect of additives on 2D perovskite film towards efficient and stable solar cell," Chem. Eng. J. **389**, 124266 (2020).
36. T. M. Koh, V. Shanmugam, J. Schlipf, L. Oesinghaus, P. Müller-Buschbaum, N. Ramakrishnan, V. Swamy, N. Mathews, P. P. Boix, and S. G. Mhaisalkar, "Nanostructuring mixed-dimensional perovskites: a route toward tunable, efficient photovoltaics," Adv. Mater. **28**(19), 3653–3661 (2016).
37. C. Ma, C. Leng, Y. Ji, X. Wei, K. Sun, L. Tang, J. Yang, W. Luo, C. Li, Y. Deng, S. Feng, J. Shen, S. Lu, C. Du, and H. Shi, "2D/3D perovskite hybrids as moisture-tolerant and efficient light absorbers for solar cells," Nanoscale **8**(43), 18309–18314 (2016).
38. Y. Zhao, A. M. Nardes, and K. Zhu, "Mesoporous perovskite solar cells: Material composition, charge-carrier dynamics, and device characteristics," Faraday Discuss. **176**, 301–312 (2014).
39. D. Cui, Z. Yang, D. Yang, X. Ren, Y. Liu, Q. Wei, H. Fan, J. Zeng, and S. Liu, "Color-tuned perovskite films prepared for efficient solar cell applications," J. Phys. Chem. C **120**(1), 42–47 (2016).
40. B. El Cohen, M. Wierzbowska, and L. Etgar, "High efficiency and high open circuit voltage in quasi 2D perovskite based solar cells," Adv. Funct. Mater. **27**(5), 1604733 (2017).
41. G. Chai, S. Luo, H. Zhou, and W. A. Daoud, "$CH_3NH_3PbI_{3-x}Br_x$ perovskite solar cells via spray assisted two-step deposition: Impact of bromide on stability and cell performance," Mater. Des. **125**, 222–229 (2017).
42. L. Atourki, E. Vega, B. Marí, M. Mollar, H. Ait Ahsaine, K. Bouabid, and A. Ihlal, "Role of the chemical substitution on the structural and luminescence properties of the mixed halide perovskite thin $MAPbI_{3-x}$ Br_x ($0 \le x \le 1$) films," Appl. Surf. Sci. **371**, 112–117 (2016).
43. F. Guo, B. Zhang, J. Wang, H. Bai, R. Guo, Y. Huang, and P. Ren, "Facile solvothermal method to synthesize hybrid perovskite $CH_3NH_3PbX_3$ (X = I, Br, Cl) crystals: publisher's note," Opt. Mater. Express **8**(2), 210 (2018).
44. Y. Lv, Y. Shi, X. Song, J. Liu, M. Wang, S. Wang, Y. Feng, S. Jin, and C. Hao, "Bromine doping as an efficient strategy to reduce the interfacial defects in hybrid two-dimensional/three-dimensional stacking perovskite solar cells," ACS Appl. Mater. Interfaces **10**(37), 31755–31764 (2018).
45. J. W. Lim, H. Wang, C. H. Choi, H. Kwon, L. N. Quan, W. T. Park, Y. Y. Noh, and D. H. Kim, "Self-powered reduced-dimensionality perovskite photodiodes with controlled crystalline phase and improved stability," Nano Energy **57**, 761–770 (2019).
46. J. Chen, J. Y. Seo, and N. G. Park, "Simultaneous improvement of photovoltaic performance and stability by in situ formation of 2D perovskite at $(FAPbI_3)_{0.88}(CsPbBr_3)_{0.12}$/CuSCN interface," Adv. Energy Mater. **8**(12), 1702714 (2018).
47. D. Bae, A. Palmstrom, K. Roelofs, B. Mei, I. Chorkendorff, S. F. Bent, and P. C. K. Vesborg, "Tailoring Mixed-Halide, Wide-Gap Perovskites via Multistep Conversion Process," ACS Appl. Mater. Interfaces **8**(23), 14301–14306 (2016).
48. Z. Liang, S. Zhang, X. Xu, N. Wang, J. Wang, X. Wang, Z. Bi, G. Xu, N. Yuan, and J. Ding, "A large grain size perovskite thin film with a dense structure for planar heterojunction solar cells via spray deposition under ambient conditions," RSC Adv. **5**(74), 60562–60569 (2015).
49. B. El Cohen, M. Wierzbowska, and L. Etgar, "High efficiency quasi 2D lead bromide perovskite solar cells using various barrier molecules,," Sustain. Energy Fuels **1**(9), 1935–1943 (2017).
50. T. Zhao, C. C. Chueh, Q. Chen, A. Rajagopal, and A. K. Y. Jen, "Defect Passivation of Organic-Inorganic Hybrid Perovskites by Diammonium Iodide toward High-Performance Photovoltaic Devices," ACS Energy Lett. **1**(4), 757–763 (2016).